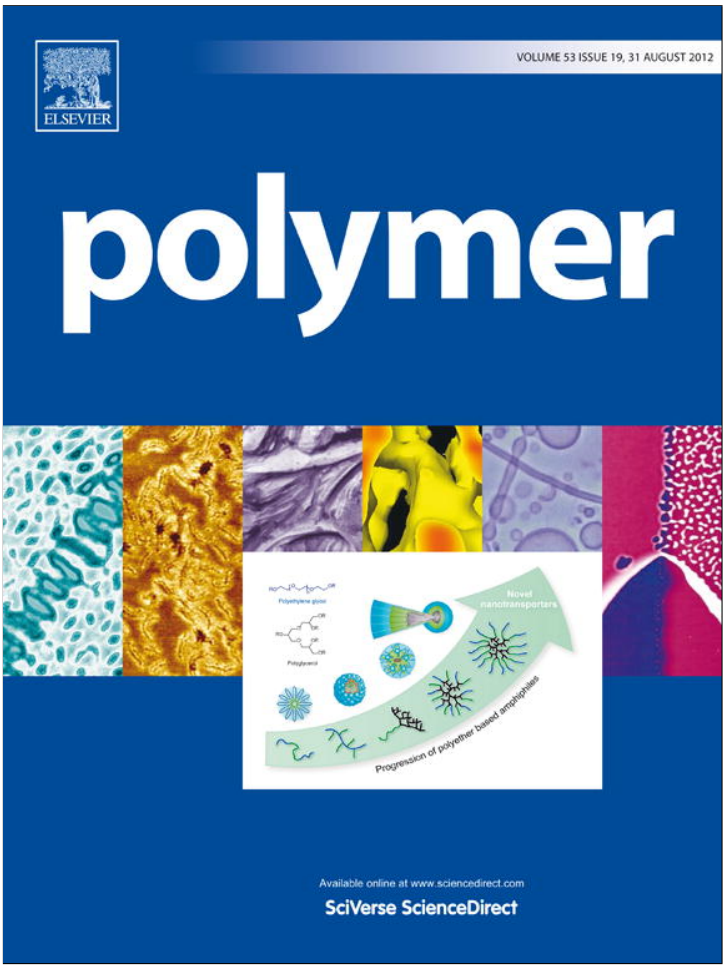

Polymer 53 (2012) 4045–4053

Contents lists available at SciVerse ScienceDirect

Polymer

journal homepage: www.elsevier.com/locate/polymer

Nanodiamond-mediated crystallization in fibers of PANI nanocomposites produced by template-free polymerization: Conductive and thermal properties of the fibrillar networks

Emanuela Tamburri [a,*], Valeria Guglielmotti [a], Silvia Orlanducci [a], Maria Letizia Terranova [a], Daniela Sordi [a,c], Daniele Passeri [b], Roberto Matassa [b], Marco Rossi [b]

[a] Dip.to Scienze e Tecnologie Chimiche – MinimaLab, Università degli Studi di Roma "Tor Vergata", Via Della Ricerca Scientifica, 00133 Roma, Italy
[b] Dip.to di Scienze di Base e Applicate per l'Ingegneria e Centro di ricerca per le Nanotecnologie applicate all'Ingegneria – CNIS, Università degli Studi di Roma "Sapienza", Via A. Scarpa, 00161 Roma, Italy
[c] Dept. of Biotechnology, Biocatalysis and Organic Chemistry, University of Technology, Julianalaan 136, 2628 BL Delft, Netherlands

ARTICLE INFO

Article history:
Received 9 March 2012
Received in revised form
20 June 2012
Accepted 8 July 2012
Available online 25 July 2012

Keywords:
Nanodiamond
Polyaniline polymerization mechanism
Fibers

ABSTRACT

The detonation nanodiamond is a novel versatile nanomaterial with tunable properties and surface chemistry. In this work, we report on a template-free method to synthesize polyaniline based nanocomposite fibers during a chemical oxidative precipitation polymerization where the cooperative interactions between nanodiamond and polyaniline nucleates trigger the final morphology of the nanocomposite. FE–SEM and TEM observations evidence the prominent growth of fibril-like structures assembled in 2-D networks of tightly woven, partially oriented fibers. Optical and Raman spectroscopy and X-ray diffraction analyses reveal that the polymer chains are in a protonated emeraldine form and organize themselves in a highly ordered 3-D spatial arrangement. Conductivity measurements performed on isolated fibers by a conductive tip of an AFM apparatus highlight that the diamond filler does not affect the conductive properties of the polyaniline matrix while increases the thermal stability of the polymer as confirmed by TGA studies.

1. Introduction

Conductive polymers (CP) are examples of functional materials that show various highly specific and desirable physicochemical properties, *in primis* in the field of charge transport. Due to their special conduction mechanism, to the reversibility of doping/dedoping processes, to the tunability of the chemical and electrochemical characteristics, a variety of conducting polymers have recently been investigated for applications in the areas of nanoscience and nanotechnology [1]. In particular, special attention received CP arranged in 1-D nanostructures, such as tubules and fibers. By now, numerous publications have demonstrated that these one-dimensional polymer structures are promising materials for fabricating polymeric devices such as chemical and bio-sensors, field-effect transistors, field emission and electrochromic display devices, supercapacitors, *etc.*, and exhibit clear advantages over their bulk counterparts in many types of applications [1]. However, in order to fulfil the potential applications of these 1-D structures, it is necessary to precisely address their physical properties. The CP conduction is indeed ascribed prevalently to charge carriers, such as polarons and bipolarons, and is thought to occur along a CP chain, between adjacent chains, among fibers and/or globules formed by the aggregated chains. In this view, it is therefore intuitive how the conductive pathways are related to the structural organization of the polymers units in the final material. On the other hand, insufficient thermal stability and poor mechanical properties constitute obvious disadvantages for functional applications of the entire class of CP [2]. Due to the intrinsic difficulties faced in processing these exciting materials, a lot of work has been thus devoted in the last decades to develop innovative synthesis methodologies and to find suitable fillers for the CP-based composites production. It is indeed well known from decades that the fillers can effectively modify the mechanical properties of the conductive polymers. However, with the development of nanotechnology, also more sophisticated applications have taken advantage from the insertion of foreign nanostructured species inside CP matrices. Nanocomposites based on conductive polymers are presently manufactured for a variety of applications: energy

* Corresponding author. Tel.: +39 (0)672594402; fax: +39 (0)672594328.
E-mail address: emanuela.tamburri@uniroma2.it (E. Tamburri).

0032-3861/$ – see front matter © 2012 Elsevier Ltd. All rights reserved.
http://dx.doi.org/10.1016/j.polymer.2012.07.014

storage devices, photovoltaic systems, sensors, electromechanical engineering, EMI shielding materials and so on [3–8]. As a general rule, the fillers have been viewed up to now as agents able to modify some functional properties of the CP matrix. Marked changes are usually detected in the characteristics of the nanocomposites, especially in the case of efficient interactions between nanoparticles and conductive polymer. The functional modifications are effective only if some specific requirements are satisfied. The first one is the reduced size and a narrow size distribution of the nanoparticles. Moreover the interactions must assure uniform dispersion and immobilization of the nanofiller in the matrix, in order to prevent particle aggregation. However, under such conditions, the spatial control and dispersion of individual nanoobjects can also be utilized to control the organization of the polymer segments, as we also observed in our previous studies dealing with the use of nanosized diamond as filler of polyaniline systems [9]. In comparison to other CP, polyaniline (PANI) is known for being a polymer easy to synthesize, at low cost and with high yield. Moreover, it has great potential for modification of the molecular structure, and undergoes a special proton doping mechanism. These unique properties lead PANI to be one of the more outstanding conducting polymers and the most promising for potential applications in technology [3,10].

In the exciting continuous research for a way to produce one-dimensional CP nanocomposite materials, in the present work we have adopted a template-free method to synthesize PANI fibers during chemical oxidative precipitation polymerization. The idea underlying this study was to exploit the cooperative interactions between the polymer segments and the diamond nanoparticles as basic driving force for the self-assembly process of the polymeric fibers. Several stimulating results were obtained from deep investigations carried out by using electron and atomic force microscopy, μ-Raman spectroscopy and X-ray diffraction. The adopted synthesis approach allowed us to produce composite fibers characterized by a remarkable high crystalline quality of the polymer matrix, the thermal stability of which turned out to be rather improved by the inclusion of the diamond filler. Nevertheless, a drawback that would make useless to utilize the diamond particles for providing a mechanically robust and thermally more stable but still conductive material, could in case arise from the insulating properties of the diamond. Conversely, it has been shown by measurements on single fibers achieved by an AFM metallic tip that the conductive properties of the polymer have not been compromised by the presence of diamond particles. All these findings lead us to consider that the PANI–DND fibers possess all those features which make them promising candidate for the realization of advanced polymeric devices.

2. Experimental

The PANI–DND composite materials were prepared by precipitation polymerization of aniline monomer in the presence of diamond nanoparticles. Purified DND particles with a 4–5 nm size, manufactured and preliminary treated by the Federal Research and Production Centre “Altai” (Russia), were used after further chemical–physical processing steps, necessary to avoid re-aggregation of the primary nanoparticles. Aniline (Fluka) was distilled under reduced pressure before use. An anionic surfactant, *i.e.* sodium dodecyl sulfate (SDS) (Sigma), was used to facilitate the DND dispersion in the aqueous reaction environment. A proper amount of SDS was therefore dissolved in a 1 M HCl (Sigma) solution where DND (500 mg) and aniline (5 mmol) were then added and sonicated for 30 min allowing the aniline monomers to adsorb on the diamond particles. Upon stirring, 1 M HCl solution containing 5 mmol ammonium persulfate (Sigma) was slowly added to the above mixture, cooled to 0–5 °C, and then kept in a polymerization. After the addition was completed, the stirring was continued for at least 6 h. The same protocol was used to prepare the composite material and the pure polymer, omitting the addition of DND in this last case. In both the preparations, the resulting reaction products were filtered and washed successively with 1 M HCl, water and ethanol until the filtrate was colorless, and then dried at 50 °C overnight under vacuum.

The prepared samples were investigated by means of different characterization techniques.

A FIB–SEM Cross Beam Workstation ZEISS Auriga and a Hitachi H-7100 transmission electron microscopy (TEM) were utilized to analyze the morphology of the samples.

The chemical structure of the polymer was investigated by Raman spectroscopy by using a Renishaw MicroRaman System 1000. Three excitation wavelengths were used: 514 nm (Spectra Physics Ar^+ laser), 633 nm (Spectra Physics He–Ne laser) and 785 nm (Renishaw diode laser).

The study of the crystalline structure was performed by X-ray diffraction (XRD). The XRD patterns were recorded using a Seifert-XRD3003 diffractometer with a Bragg–Brentano geometry, employing a Cu Kα source ($\lambda = 1.54056$ Å).

Atomic force microscopy (AFM) was used to study the fibers topography and to perform local electrical characterization and mapping. The apparatus (Solver, NT-MDT, Russia), operating at room conditions, was equipped with commercial Si cantilevers (NSG10, NT-MDT, Russia) for the topographical characterization in standard semi-contact mode. The electric characterization was performed using commercial Pt coated Si cantilevers (CSG10/Pt, NT-MDT, Russia) in contact mode using the experimental configuration described below.

Optical spectra were recorded with a UV-1800 Shimadzu spectrophotometer. Optical images were acquired by a polarizing optical microscope (Zeiss Axiovert 200 MAT).

Finally, thermal properties were determined using a PerkinElmer Pyris Diamond thermogravimetric/differential thermal analyzer (TG/DTA). TGA experiments were performed under nitrogen atmosphere from 25 °C to 600 °C at a heating rate of 10 °C/min.

3. Results and discussion

As widely reported in literature, a compact granular structure is the most typical morphology of PANI produced by the precipitation in strongly acid media [11]. Accordingly to this, a powder constituted by bright green micrometer-sized grains has been obtained in the case of the pure PANI polymer prepared by the chemical oxidization of the aniline monomer in the concentrated HCl aqueous solution (Fig. 1).

Under the adopted experimental conditions the presence of the SDS surfactant seems not to affect the self-assembly of aniline nucleates as demonstrated in other experiments [12–17]. Different results are found when the DND particles are used as additional reagent. First, the introduction of the DND particles into the reaction mixture makes the polymerization rate faster, as observed through the very rapid color change of the reaction medium from light gray to blue. Second, the presence of the diamond reagent induces a conversion from granular to one-dimensional morphology of PANI, as evinced in the optical micrographs of the produced material (Fig. 2). It can be observed that the PANI–DND composite is constituted by a tightly woven network of fibers (Fig. 2a) which are characterized by a length of several microns (Fig. 2b), and which in some case seem to be branched. Moreover, the image recorded using the reflected dark-field observation method (Fig. 2c) reveals that the fibers present some surface roughness.

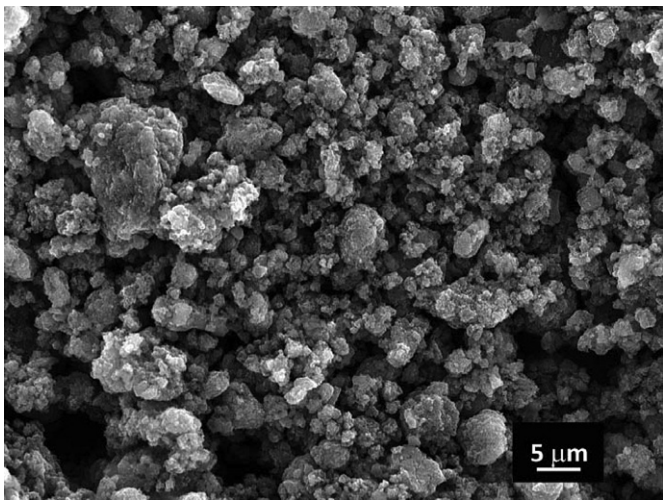

Fig. 1. SEM image showing the granular morphology of the pure PANI powder prepared by the chemical oxidization of the aniline monomer in the concentrated HCl aqueous solution.

Atomic force microscopy (AFM) studies allowed us to perform an accurate analysis of the morphology of such structures, that appear indeed constituted by bundles of tubular fibrils with diameter approximately in the range 300–500 nm (Fig. 3a). It derives that the fibers essentially result from a two dimensional assembling of such fibrils and show sizes in the range 300–500 nm (thickness) and 1–3 μm (width) (Fig. 3b).

The feature of the fibers is better detailed in the TEM images where their multi-fibrillar nature is evidenced (Fig. 4a). Moreover the TEM pictures show that the surfaces of fibrils are definitely characterized by a globular morphology responsible for the typical roughness to the final fibers (Fig. 4b).

All these results are in agreement with our previous assumption of a "seeding" induced by DND, able to influence the process of nanofiber nucleation during electrochemical polymerization [9] and indicate a similar seeding effect is active also in the case the chemical polymerization. The explanation of such capability has to take into consideration several aspects. First of all, it can be reasonably assumed that diamond nanoparticles offer supplementary surfaces for the polymer nucleation. Moreover, the facet-dependent variations of the surface electrostatic potential shown by these particles [18] can play a fundamental role in the primary interactions involved in the self-assembling process that leads to one-dimensional polymeric systems. In this view, the multi-pole structure of the DND particles can govern the interactions of the facets with the polymer nucleates in a way that resembles what occurs in the soft-template synthesis of CP fiber structures [2]. A detailed analysis of the chemical and structural characteristics of these fascinating PANI–DND hybrid systems becomes anyway necessary in order to relate them to the functional properties possibly shown by the material. In fact the key point to be considered in using CP-based materials is that the conduction of these systems is highly dependent on both the chemical oxidation state of the single chain and on the overall 3-D arrangement of the chains. The polaronic and bipolaronic charge carriers are associated with an oxidized state of the polymer backbone that, in the case of PANI, is known to be the protonated emeraldine form. The motion of such carriers along a backbone and the hopping among neighboring backbones and among fibers or globules, contributes to the conduction through all the material [19]. The conduction model associated with this situation is usually depicted by considering the existence of conductive islands, which are crystalline regions of polymer where the chains are orderly arranged, and which are embedded in the not conductive amorphous polymer phase

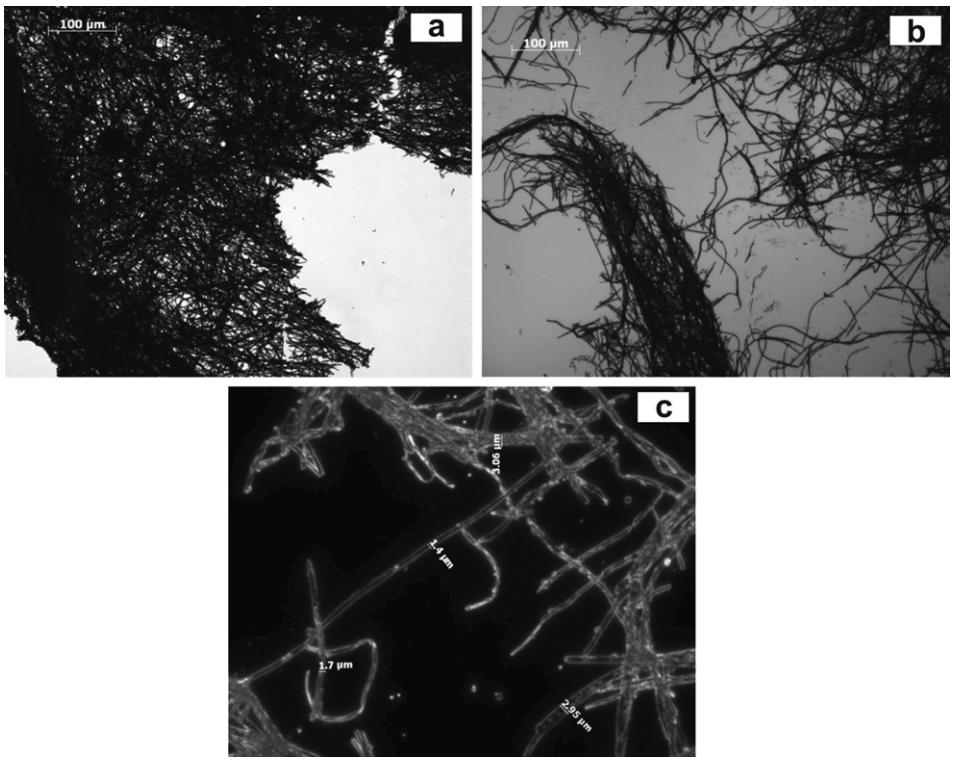

Fig. 2. Network of PANI–DND fibers observed by optical microscope in (a) transmission, (b) reflection, and (c) reflection dark-field illumination method.

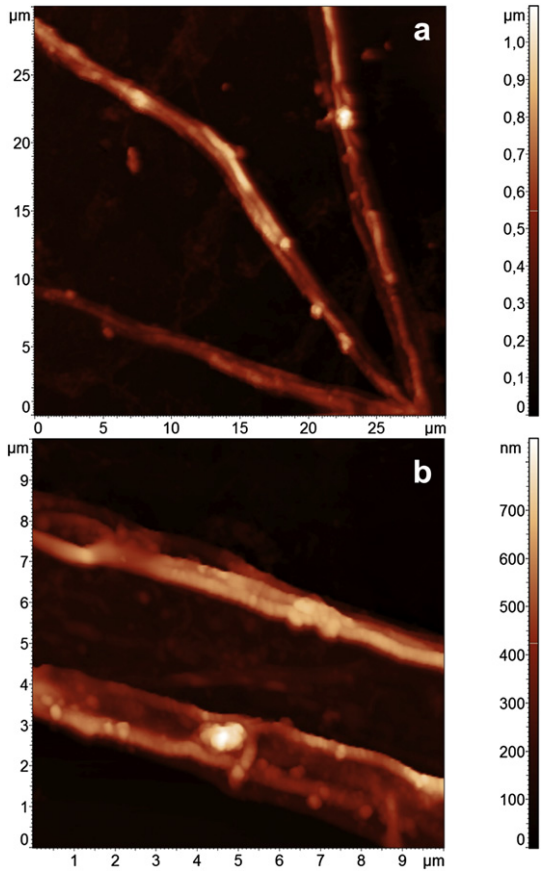

Fig. 3. AFM images showing (a) the multi-fibrillar nature and (b) the morphology of the PANI–DND fibers.

[19,20]. It follows that in this perspective is crucial to assess both the state of oxidation and the spatial organization of the polymer chains when the growth and the arrangement of the PANI chains is triggered by the presence of DND fillers.

Information at molecular level of the polymer chains properties has been achieved by optical and Raman spectroscopy. In Fig. 5 the optical spectra of PANI and PANI–DND samples are presented.

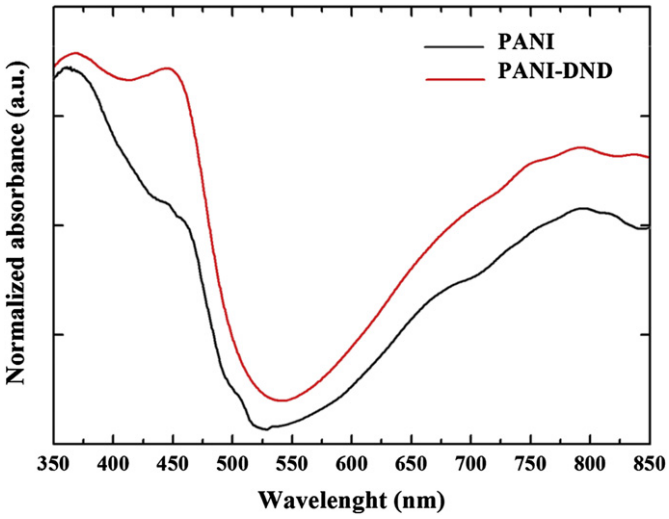

Fig. 5. Optical spectra of PANI powder and PANI–DND composite fibers.

Three significant peaks can be clearly distinguished at ca. 363 nm, 445 nm and 790 nm. The first peak corresponds to the $\pi-\pi^*$ transition, while the last two signals correspond to the electron transitions from the π valance band to the polaronic levels characteristic of the doped emeraldine oxidation state of PANI, *i.e.* the protonated emeraldine form [21–23]. Moreover a shoulder can be detected at about 675 nm. This signal, more evident in the pure PANI spectrum, can be associated with charge transfer transitions from benzenoid to quinonoid rings present along the PANI backbone [23].

As a consequence, a coexistence of benzenoid and quinonoid type structures is found in the polymer main chains of both pure and nanocomposite materials. Since the enhancement of the modes originating from the vibrations of benzenoid and quinonoid segments depends on the excitation line wavelength, the presence of such structures can be confirmed by the Raman analysis carried out with different excitation sources [23]. Raman spectra obtained with the three excitation lines 514, 633, and 785 nm respectively are shown in Fig. 6. In Table 1 a tentative assignment of all the Raman bands is reported.

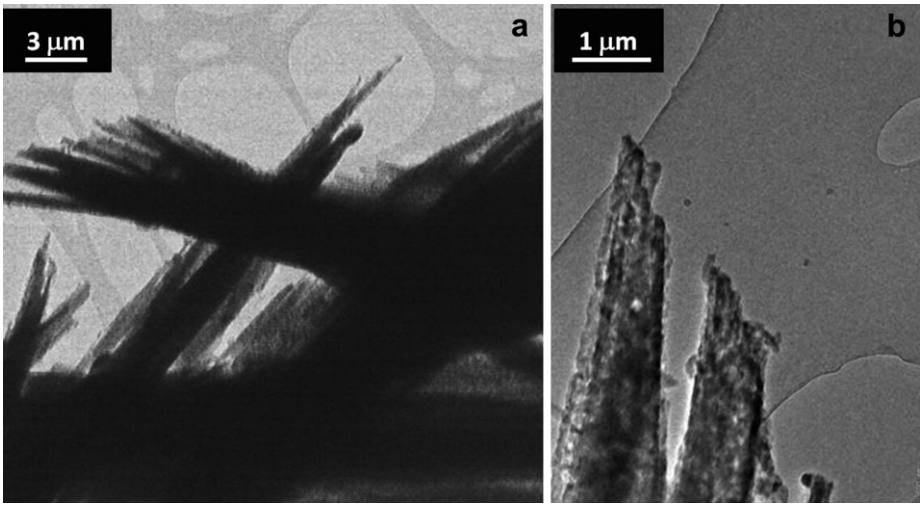

Fig. 4. TEM micrographs revealing (a) the two dimensional assembling and (b) the globular morphology of PANI–DND fibrils.

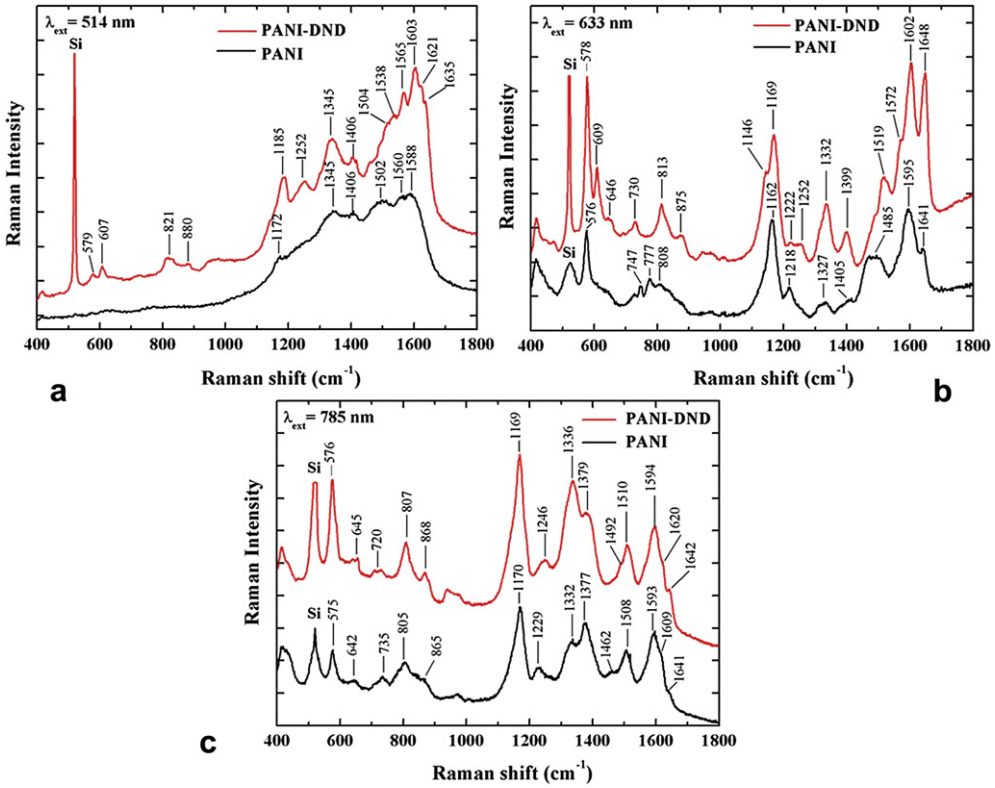

Fig. 6. Raman spectra of PANI and PANI–DND taken using (a) 514 nm; (b) 633 nm; and (c) 785 nm excitation wavelength.

Table 1
Assignments of the Raman bands for PANI and PANI–DND. Excitation wavelength: 514, 633 and 785 nm.

λ_{exc} = 514 nm		λ_{exc} = 633 nm		λ_{exc} = 785 nm		Assignments	References
PANI	PANI–DND	PANI	PANI–DND	PANI	PANI–DND		
	579	575	576	576	578	Pho, B ring def.	[24–29]
	607		609			υ (C–S), δ (SO_2) Benz. ring def. (i.p.)	[24,30–32]
			646	642	645	Benz. ring def. (i.p) (*para*-)(6*b*) υ (C–S), δ (SO_2)	[24,31–33]
			730		720	C–C ring def. (o.p.), Phz	[24,30,34]
				735		Q ring def. (o.p.), Phz	[24,28,33,34]
		747				Ring bend. (o.p.)(Q)	[24,30]
		777				Q ring def.	[35,36]
			808	805	807	C–H def. (o.p.), ring def. SQ	[24,30,33,37]
	821	813				δ $(C–H)_Q$(o.p.)	[24,30]
				865	868	B ring def. (i.p)	[24,33]
	880		875			δ (C–H) (o.p.)	[24,38]
1172		1162	1169	1170	1169	δ $(C–H)_{SQ}$(9*a*)	[37,39–41]
	1185					δ $(C–H)_B$	[23,41,42]
		1218	1222	1229		υ $(C–N)_B$, Phz	[24,43,44]
	1252		1252		1246	υ $(C–N)_B$	[43,45,46]
1345	1345	1327	1332	1332	1336	υ $(C\sim N^{+\bullet})$	[24,47–49]
				1377	1379	υ $(C\sim N^{+})$ Saf	[34,48,50]
1406	1406	1405	1399	1405	1399	Phz	[24,51,52]
		1485				υ $(C{=}N)_Q$ Phz	[49,53]
1502	1504		1519	1508	1510	δ $(N–H)_{SQ}$	[24,51,54,55]
1560	1565		1572			υ $(C–C)_q$, Phz	[34,45,56]
1588		1595		1593	1594	υ $(C{=}C)_Q$(8*a*)[a]	[30,47,48]
						υ $(C\sim C)_{SQ}$(8*b*)[a]	[36,40,44,57]
	1603		1602	1609		υ $(C–C)_B$	[47,57,58]
	1621s				1620	υ $(C\sim C)_B$(8*a*)[a]	[30,37,42,47,48]
	1635s	1641s	1648	1641s	1642	υ $(C\sim C)_B$(8*a*)[a], Phz	[34,50–52]

B, benzenoid ring; Q, quinonoid ring; υ stretching; δ, in-plane bending; ∼, bond intermediate between the single and the double bonds; Phz, phenazine-like segment.
[a] Wilson notation for aromatic species modes.

The spectral regions of interest for PANI backbone structure analysis are: (1) the 1650–1400 cm^{-1} range relative to C∼C stretching vibrations of benzenoid (B) and quinonoid (Q) rings and to C═N stretching in quinonoid units and (2) the 1400–1200 cm^{-1} range relative to stretching vibrational modes of charged nitrogen segments [24]. The signals located between 1650 and 1600 cm^{-1} can be attributed to the C∼C vibrations of B ring mixed with the ring-stretching vibrations of substituted phenazine segments [24]. They appear as a broad band in the PANI–DND spectrum recorded with the green line (Fig. 6a) and as a shoulder in the spectra of PANI and PANI–DND acquired with the near-infrared line (Fig. 6b). Two distinct peaks at 1602 and 1648 cm^{-1} and only a shoulder at 1641 cm^{-1} are clearly visible in spectra recorded with the red line for PANI–DND and PANI, respectively. On the other hand, the signal associated with the C∼C stretching of semiquinonoid radical structures typical of the protonated emeraldine form of PANI is present as a relative strong band at ca. 1594 cm^{-1} in the spectra of both PANI and PANI–DND recorded with the 785 nm light. The signal ascribed to the C═N stretching is clearly viewed as a broad band at 1458 cm^{-1} in the PANI spectrum acquired with the 633 nm, whereas the "polaronic band" corresponding to the υ (C∼$N^{+\bullet}$) vibration of the polaronic structures is found in the various spectra at positions varying from 1332 to 1345 cm^{-1}. The wavenumber of this mode is sensitive to electron delocalization around the C∼N∼C part of the polymer backbone and it is typically lower for a more delocalized structure, *i.e.* radical segments with a larger conjugation length [25,26]. Comparing the position of this mode in the spectra obtained with the red and NIR lines, it seems that PANI in the composite fibers is characterized by polarons with conjugation lengths slightly shorter than in the pure polymer. Finally, the presence of the strong band at ca. 1169 cm^{-1} due to the δ (C–H) vibration of the semiquinonoid rings in the spectra of PANI and PANI–DND recorded with the 633 and 785 lines definitively demonstrates the conductive protonated emeraldine oxidation state of the PANI main chain both in the pure polymer and in the composite fibers. In particular, a higher protonation level seems to be present in the second case. In fact, a closer look at the results reveals that the signals ascribable to quinonoid like segments are present at a higher extent in all the spectra recorded for the pure PANI sample (Table 1). As a conclusion we can derive that the more localized polaronic structures found for the polymer in the composite fibers are anyway counterpoised by a larger number of these conductive regions than those present in the pure polymer.

The crucial further step for a complete understanding of the fibers structures is to evaluate whether the packing of the polymeric chains leads to the formation of a long-range order even into these interesting one-dimensional systems. At this aim, X-ray diffraction (XRD) experiments have been performed on PANI–DND samples and, for a comparison, on the pure polymer. The XRD spectra of PANI and PANI–DND are presented in Fig. 7a and b respectively.

For pure PANI (Fig. 7a), the peaks appearing at 9.14°, 14.85°, 20.26° and 25.32° correspond to (001), (011), (020), and (200) reflections of the protonated emeraldine form [59,60]. The crystal plane (d_{hkl}) corresponding to every peak is reported in the diffractograms and in Table 2.

In the XRD spectrum acquired from the PANI–DND fibers, all the diffraction peaks present in the pure polymer spectrum are observed. Anyway it is worth to highlight that, in the case of the composite fibers, it is possible to discriminate also two additional peaks at 27.13° and 29.60°, corresponding respectively to the (121) and (022) reflections of the polymer structure. Furthermore, the clear presence of the three main reflections of cubic diamond confirms that the synthesis process has been able to insert the DND particles in the polymeric network, without interfering with the growth of the conducting polymer that still retains its crystalline structure [61]. A more comprehensive structural analysis can be performed by analyzing the two sharp peaks having the highest intensity in the spectra of both PANI and PANI–DND. These peaks are located at $2\theta = 20.26°$, corresponding to the d_{020} crystal plane (the periodicity along the polymer chain) and at $2\theta = 25.32°$ corresponding to the d_{200} crystal plane (the periodicity perpendicular to the polymer chain). For each peak the analysis of width and intensity gives indications about the size distribution and amount of the polymer crystallites for a particular crystal plane [62]. Both for PANI and PANI–DND the X-ray spectra indicate that the majority of crystallites layout along the direction of the d_{200} crystal plane. This result is of particular interest considering the model proposed for the structure of the PANI nanofibers [10]. It is assumed that, under favorable conditions, the aniline nucleates produce stacks from which PANI chains perpendicularly grow producing the body of a nanofiber. As a consequence, the radius of the nanofiber is proportional to the length of the PANI chains growing from its center. Moreover, it has been proven that the enhancement of the conductivity is a result of the orientation of the polymer chains in a direction perpendicular to the nanofiber axis [63]. The observed large number of crystallites aligned along the direction perpendicular to the polymer chain reveals that the chains are orderly arranged in the direction perpendicular to the nanofiber axis. Assuming valid the model of the nanofiber structure, a structure as that depicted in the SEM image of Fig. 8 and a conductive form are therefore expected for the fibers constituted by the PANI–DND nanofibrils.

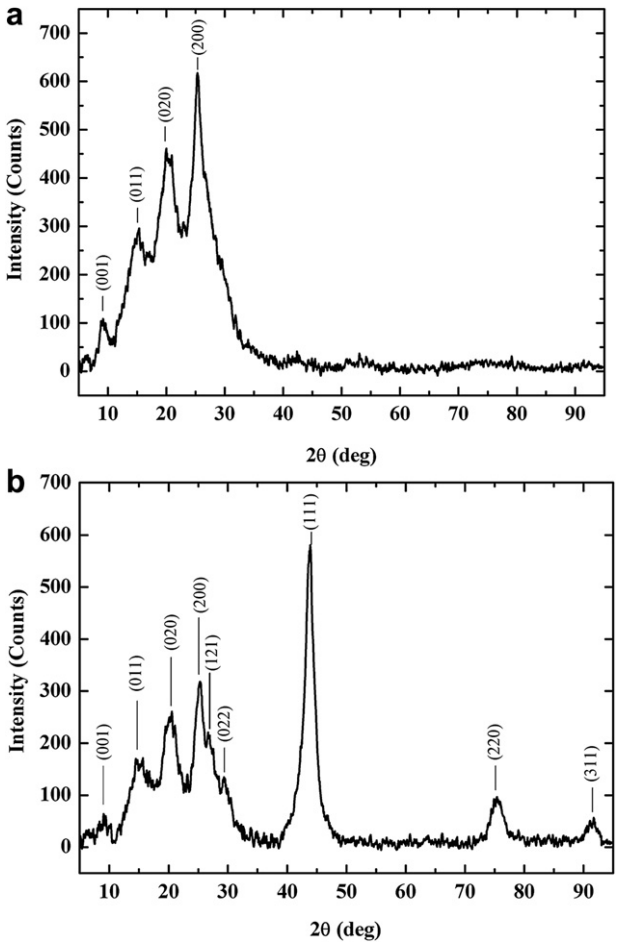

Fig. 7. XRD patterns of PANI (a) and PANI–DND (b) indicating the main reflections.

Table 2
Assignments of the XRD peaks for PANI and PANI–DND.

PANI	PANI–DND	Assignments
9.14	8.93	d_{001} *p*
14.85	15.06	d_{011} *p*
20.26	20.30	d_{020} *p*
25.32	25.16	d_{200} *p*
	27.13*	d_{121} *p*
	29.60*	d_{022} *p*
	43.77	d_{111} *d*
	75.46	d_{220} *d*
	91.40	d_{311} *d*

p, polymer; *d*, diamond; *, additional polymer peaks.

So far, spectroscopic and structural analyses demonstrated that the polymeric component of the composite fibers possesses a chemical and structural form compatible with a conductive state. Nevertheless, it was felt worthwhile to perform conductivity measurements in order to verify that the host PANI has really maintained its conducting properties with the not conducting DND particles as filler. The strategies for estimating or measuring the electrical conductivity of individual fibers typically comprise the two-probe or the four-point conductivity measurements of compressed pellet or films of the polymer fibers [1]. However these approaches cannot exclude the inter-fiber contact resistance, which may be larger than the intrinsic resistance of the polymer fibers and even dominate the measured resistance of the compressed pellet or film [64,65]. In such a context, we considered more appealing to test directly the conduction of the individual fibers. AFM characterization has been therefore carried out on isolated PANI–DND fibers (Fig. 9).

An Ag electrode was realized at one end of the fibers network. The sample was then imaged in contact mode by applying a dc voltage ΔV between this electrode and the tip and acquiring the current flowing from the tip to the sample (Fig. 9a). The current signal was recorded at each point of the scanned area simultaneously with the morphological reconstruction of the sample, thus enabling the creation of a current map.

The AFM images and the corresponding current maps obtained by applying $\Delta V = 2$ V between the AFM tip and two isolated PANI–DND fibers are shown in Fig. 9b and c respectively. The current map clearly demonstrates the flowing of electric current in

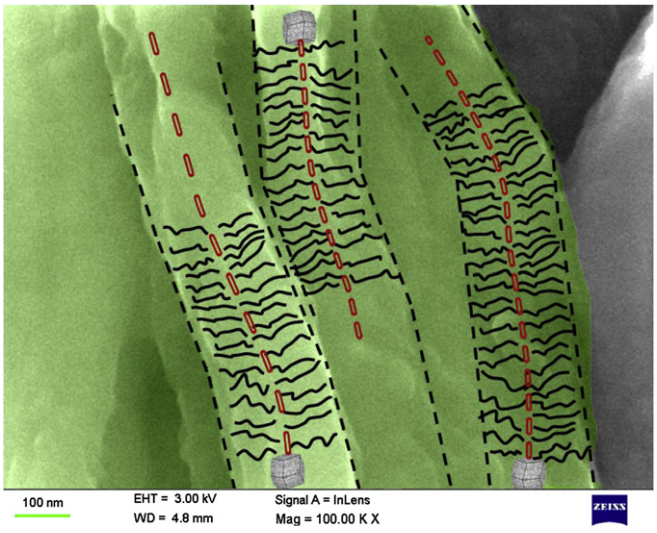

Fig. 8. SEM image reporting a schematic illustration of the nanofibrils constituting a PANI–DND fiber.

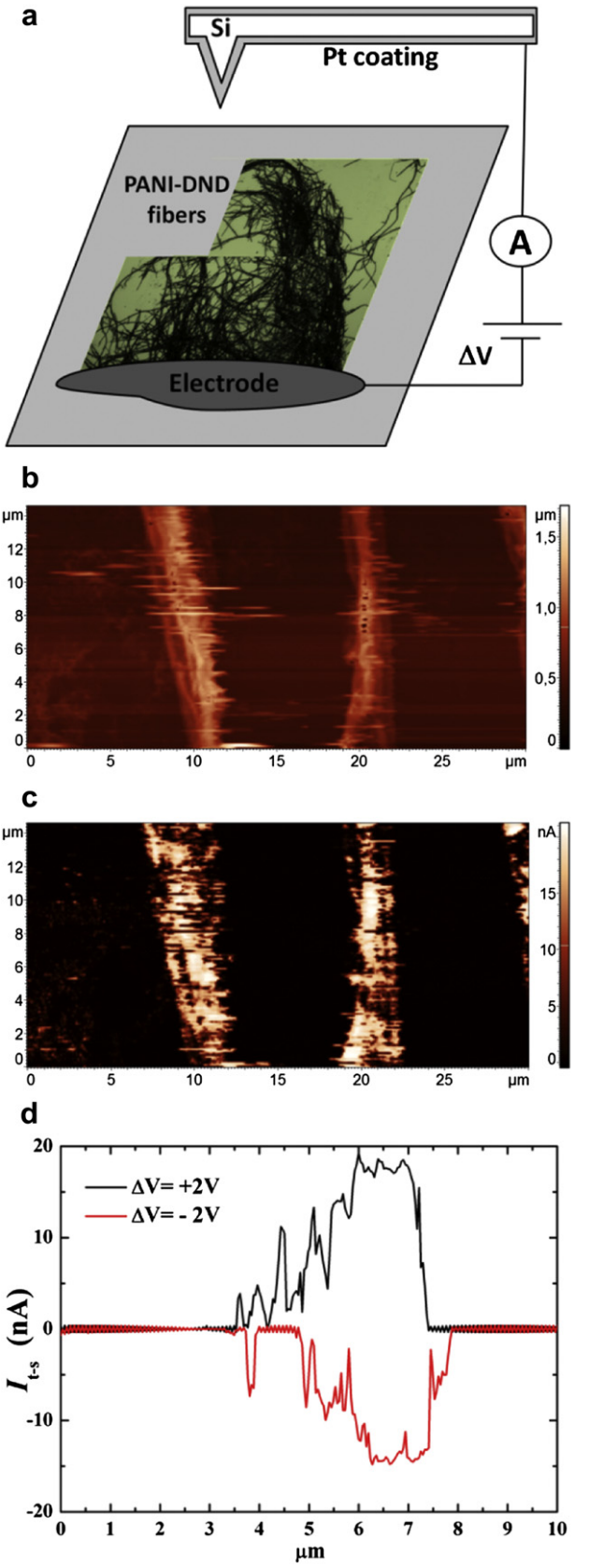

Fig. 9. Conductivity imaging of individual PANI–DND fibers: (a) schematic diagram of the measuring method based on a conductive Pt tip of an AFM apparatus; (b) AFM image and (c) current maps of two isolated PANI–DND fibers; (d) current I_{t-s} flowing from tip to PANI–DND fibers sample recorded at each point of the scanned area.

correspondence of the fibrils constituting the fibers, while no current signal above the noise is collected in correspondence of the substrate and the inversion of the direction of the electric current flow is observed when the sign of ΔV reverses (Fig. 9d). A rough estimation of the conductibility of a single PANI fiber gives σ values as high as a few hundreds of S/m, that are well within the range measured in other similar experiments on pure PANI fibers [1,66,67]. Note that such a parameter represents the PANI–DND fiber conductibility along its long axis direction, since the experimental configuration used for the measurements does not allow the access to the direction normal to the main axis. However the results uncontrovertibly demonstrate that the PANI–DND fibers are conductive and that the insertion of the DND particles inside the PANI matrix does not significantly affect the charge transport properties of the conducting polymer.

At this point it is essential to remind that one of the major benefits expected from the integration of diamond systems with PANI is undoubtedly an increase in thermal performance of the final composite material. At this aim thermo-gravimetric analysis has been adopted to evaluate the onset decomposition temperatures, and determine the thermal stability of PANI and PANI–DND samples. The experimental diagrams relative to PANI, DND nanoparticles, and PANI–DND composite fibers are presented in Fig. 10.

The TGA profile of the pure polymer shows, according to literature, a decomposition process occurring in three steps. The first one, between 30 °C and 100 °C, is mainly due to some volatile matter and absorbed moisture. The second step, 150–300 °C, is ascribable to loss of bound water molecules acting as secondary dopant. Finally, between 400 and 600 °C, it is possible to observe the oxidative degradation of PANI chains [68,69]. Nanodiamonds are well-known to be thermally stable. Oxidation of nanodiamond is usually observed at temperatures higher than 800–900 °C. The oxidation of the amorphous C sp^3 phase and of graphite-like material, characterized by the presence of mixed types of hybridization (sp^2 and sp^1), occurs at approximately 550 °C. In our experiments only a 5% weight loss was observed by heating the nanodiamond particles up to 600 °C. This indicates the high level of phase purity of the nanodiamond particles used. As the pure PANI, also the PANI–DND fibers present two steps of mass loss. Noteworthy, the composite results thermally more stable than the polymer. This characteristic can be easily demonstrated by comparing the temperature relative to the weight loss. The temperatures corresponding to the weight loss of 10% (T_{10}) and 20% (T_{20}), extrapolated from the TGA curves, are used to indicate the thermal stability of PANI and PANI–DND composites. It is to be noted that a T_{10} increase from 215.3 to 239.4 °C and a T_{20} outstanding increase from 253.3 to 444.6 °C have been realized. These findings represent a further evidence of how the DND particles are intimately incorporated into the polymer matrix and how efficient this insertion is in preventing the effect of the thermal degradation of the polymer.

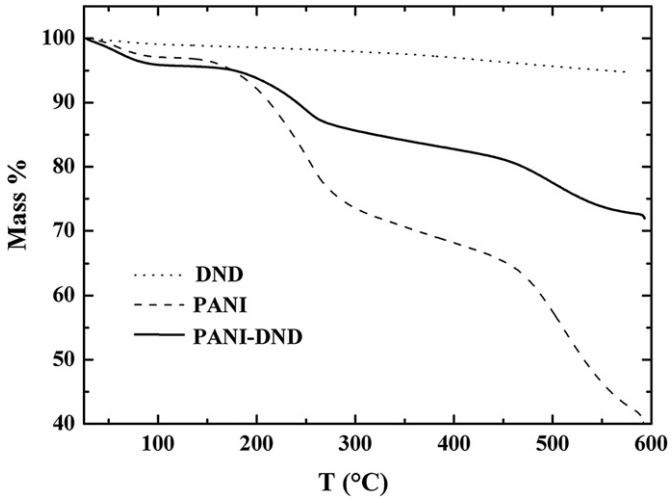

Fig. 10. TGA of PANI, DND, and PANI–DND fibers.

4. Conclusions

The present study has been focused on the preparation by precipitation polymerization and characterization of polyaniline-detonation nanodiamond composites. Networks of PANI–DND fibers constituted by bundles of fibrils have been obtained using a template-free synthesis method. The mutual layout of DND particles and the polyaniline polymer, the architectures obtained by their coupling and the effects that the DND incorporation produces on the functional properties of the nanocomposite material have been deeply investigated by using different characterization techniques. The main output is that the morphology of the polymer is highly ruled by the interactions with DND which appear as the driving forces for the self-assembly process of the one-dimensional composite structures. At molecular level, polyaniline is produced in its protonated emeraldine form whereas a high crystalline quality is found for its 3-D spatial arrangement. The structural analysis reveals for the fibers a preferential orientation of the polymer crystallites along the d_{200} crystal plane, in the direction parallel to the fiber axis according to the model proposed in literature. From the functional point of view, the first important effect of the DND presence during the material preparation step is the speed-up of the polymerization process, indicative of the high catalytic activity of such a filler. A further important effect produced by the embedding of nanodiamonds inside the polymer fibers is the noticeable increase of the thermal stability and the decrease of the temperature-induced decomposition of the PANI backbone. The research addressed to measure at the nanoscale the conductivity of the fiber nanocomposite demonstrates that the electrical properties of PANI are not affected by the insertion of the insulating diamond phase. Overall, the results of the present research suggest that the PANI–DND cooperative interactions trigger the final morphology and organization of the nanocomposites, without affecting the crystalline characteristics or the oxidative state of the PANI and therefore without modifying the charge transport properties of the nanocomposite with respect to the pure PANI. Some other outstanding properties, such as the increase of thermal stability, are added to such innovative complex nanostructures, whose realization opens new scenarios both in fundamental sciences and ultimate technological objectives.

Acknowledgment

The authors acknowledge Professor Theo Dingemans for the thermal measurements facility.

References

[1] Longa YZ, Li MM, Gub C, Wan M, Duvaild JL, Liue Z, et al. Prog Polym Sci 2011; 36:1415–42.
[2] Wan M. Macromol Rapid Comm 2009;30:963–75.
[3] Gairola SP, Verma V, Kumar L, Dar MA, Annapoorni S, Kotnala RK. Synth Met 2010;160(21–22):2315–8.
[4] Jimenez P, Demir A, Bozkurt Y, Maser WK, Saricifici NS. J Textile Institute 2011;102(10):857–62.
[5] Yoon SB, Yoon EH, Kim KB. J Power Sourc 15 December 2011;196(Issue 24): 10791–7.

[6] Sousa PM, Gutiérrez M, Mendoza E, Llobera A, Chu V, Conde JP. Appl Phys Lett 2011;99(4). art. no. 044104.
[7] Bedeloglu A, Mangu R, Rajaputra S, Singh VP. Nanotechnology 2011;22(21). art. no. 215502.
[8] Nyholm L, Nyström G, Mihranyan A, Strømme M. Adv Mater 2011;23(33): 3751–69.
[9] Tamburri E, Orlanducci S, Guglielmotti V, Reina G, Rossi M, Terranova ML. Polymer 2011;52:5001–8.
[10] Syed AA, Dinesan MK. Talanta 1991;38(No. 8):815–37.
[11] Stejskal J, Sapurina I, Trchová M. Prog Polym Sci 2010;35:1420–81.
[12] Li GC, Pang SP, Liu JH, Wang ZB, Zhang ZK. J Nanoparticle Res 2006;8: 1039–44.
[13] Langer JJ, Golczak S. Polym Degrad Stab 2007;92:330–4.
[14] Wu TM, Lin YW. Polym Eng Sci 2008;48:823–8.
[15] Zhou CQ, Han J, Guo R. J Phys Chem B 2008;112:5014–9.
[16] Zhou CQ, Han J, Guo R. Macromolecules 2009;42:1252–7.
[17] Han YG, Kusunose T, Sekino T. J Polym Sci B Polym Phys 2009;47:1024–9.
[18] Chang LY, Ösawa E, Barnard AS. Nanoscale 2011;3:958–62.
[19] Skotheim TA, Reynolds J. Handbook of conducting polymers. 3rd ed., vol. 2. CRC, ISBN 1574446657; 2007–01–16.
[20] Leite FL, Alves WF, Mir M, Mascarenhas YP, Herrmann PSP, Mattoso LHC, et al. Appl Phys A Mater Sci Process 2008;93:537–42.
[21] Zuo F, McCall RP, Ginder JM, Roe MG, Leng JM, Epstein AJ, et al. Synth Met 1989;29:E445–50.
[22] Bartonek M, Sariciftci NS, Kuzmany H. Synth Met 1990;36:83–93.
[23] Laska J, Girault R, Quillard S, Louarn G, Proń A, Lefrant S. Synth Met 1995;75: 69–74.
[24] Ćirić–Marjanović G, Trchová M, Stejskal J. J Raman Spectros 2008;39: 1375–87.
[25] Ueda F, Mukai K, Harada I, Nakajima T, Kawagoe T. Macromolecules 1990;23: 4925–8.
[26] do Nascimento GM, Temperini MLA. J Raman Spectros 2008;39:772–8.
[27] do Nascimento GM, Pereira da Silva JE, Córdoba de Torresi SI, Temperini MLA. Macromolecules 2002;35:121.
[28] Socrates G. Infrared and Raman characteristic group frequencies. New York: Wiley; 2001. p. 220–72.
[29] Brolo AG, Addison CJ. J Raman Spectros 2005;36:629.
[30] Cochet M, Louarn G, Quillard S, Boyer MI, Buisson JP, Lefrant S. J Raman Spectros 2000;31:1029.
[31] Panicker CY, Varghese HM, Anto PL, Daizy P. J Raman Spectros 2006;37:853.
[32] Anto PL, Panicker CY, Varghese HT, Philip D. J Raman Spectros 2006;37:1265.
[33] Cochet M, Louarn G, Quillard S, Buisson JP, Lefrant S. J Raman Spectros 2000; 31:1041.
[34] Durnick TJ, Wait SC. J Mol Spectros 1972;42:211.
[35] Zhang J, Liu C, Shi G. J Appl Polym Sci 2005;96:732.
[36] Boyer MI, Quillard S, Rebourt E, Louarn G, Buisson JP, Monkman A, et al. J Phys Chem B 1998;102:7382.
[37] Boyer MI, Quillard S, Louarn G, Froyer G, Lefrant S. J Phys Chem B 2000;104:8952.
[38] Harada I, Furukawa Y, Ueda F. Synth Met 1989;29:E303.
[39] do Nascimento GM, Silva CHB, Temperini MLA. Macromol Rapid Comm 2006; 27:255.
[40] Bernard MC, Hugot-Le Goff A. Electrochim Acta 2006;52:728.
[41] Kilmartin PA, Wright GA. Synth Met 1999;104:145.
[42] Quillard S, Louarn G, Lefrant S, MacDiarmid AG. Phys Rev B 1994;50:12496.
[43] Furukawa Y, Ueda F, Hyodo Y, Harada I, Nakajima T, Kawagoe T. Macromolecules 1988;21:1297–305.
[44] Cochet M, Corraze B, Quillard S, Buisson JP, Lefrant S, Louarn G. Synth Met 1997;84:757–8.
[45] Wu L-L, Luo J, Lin Z-H. J Electroanal Chem 1996;417:53–8.
[46] Shreepathi S, Holze R. Chem Mater 2005;17:4078.
[47] Louarn G, Lapkowski M, Quillard S, Pron A, Buisson JP, Lefrant S. J Phys Chem 1996;100:6998–7006.
[48] Niaura G, Ma¸eikienė R, Malinauskas A. Synth Met 2004;145:105–12.
[49] Ma¸eikienė R, Statino A, Kuodis Z, Niaura G, Malinauskas A. Electrochem Comm 2006;8:1082–6.
[50] Ćirić-Marjanović G, Blinova NV, Trchová M, Stejskal J. J Phys Chem B 2007; 111:2188.
[51] do Nascimento GM, Constantino VRL, Landers R, Temperini MLA. Macromolecules 2004;37:9373–89.
[52] do Nascimento GM, Constantino VRL, Landers R, Temperini MLA. Polymer 2006;47:6131–9.
[53] Pereira da Silva JE, de Faria DLA, Córdoba de Torresi SI, Temperini MLA. Macromolecules 2000;33:3077.
[54] Wei Z, Wan M, Lin T, Dai L. Adv Mater 2003;15:136.
[55] Tagowska M, Pałys B, Jackowska K. Synth Met 2004;142:223.
[56] Bernard MC, Hugot-Le Goff A. Electrochim Acta 2006;52:595–603.
[57] Pereira da Silva JE, Cordoba de Torresi SI, Temperini MLA. J Braz Chem Soc 2000;11:91.
[58] Quillard S, Louarn G, Buisson JP, Lefrant S, Masters J, Macdiarmid AG. Synth Met 1993;55:475–80.
[59] Dong B, He BL, Xu CL, Li HL. Mater Sci Eng B 2007;143:7–13.
[60] Chaudhari HK, Kelkar DS. Polym Int 1997;42:380–4.
[61] JCPDS–DIA. J Am Ceram Soc 1992;75:1876.
[62] Bhadra S, Kim NH, Lee JH. J Appl Polym Sci 2010;117:2025–35.
[63] Parthasarathy RV, Martin CR. Chem Mater 1994;6:1627.
[64] Mativetsky JM, Datars WR. Physica B 2002;324:191–204.
[65] Long YZ, Zhang LJ, Ma YJ, Chen ZJ, Wang NL, Zhang Z, et al. Macromol Rapid Comm 2003;24:938–42.
[66] Cai CD, Zhou JZ, Qi L, Xi YY, Lan BB, Wu LL, et al. Acta Phys Chim Sin 2005;21: 343–6.
[67] Xiong SX, Wang Q, Chen YH. Mater Lett 2007;61:2965–8.
[68] Bhadra S, Khastgi D. Synth Met 2009;159:1141–6.
[69] Qi Y, Zhang J, Qiu S, Sun L, Xu F, Zhu M, et al. J Therm Anal Calorim 2009;98: 533–7.